A Comprehensive Study of Transistors Based on Conductive Polymer Matrix Composites

Nima Sefidmooye Azar and Mahdi Pourfath, *Senior Member, IEEE*

***Abstract*— A comprehensive study is conducted on the electron transport in conductive polymer matrix composites (CPMCs), employing the nonequilibrium Green's function formalism. This paper provides a microscopic insight into the electron tunneling through the potential barriers existing between conducting sites. It is shown that Wentzel–Kramers–Brillouin approximation as well as other models with simple barrier shapes, which are widely used in literature, can lead to inaccurate results in comparison with the quantum mechanical approach using a hyperbolic barrier. In this paper, unlike most previous ones, percolation-related effects are disregarded for further focus on electron transport through the polymer potential barriers. It is assumed that a tunneling-conductive channel exists between the electrodes. This can be created either by applying electric field alignment or using a filler volume fraction higher than the percolation threshold. A two electrode resistive device is studied and the results indicate that a conductor–insulator transition occurs at a barrier thickness of ∼1.7 nm and the barrier thickness should be larger than several angstroms. Next, a novel tunneling field-effect structure based on CPMCs is introduced and its characteristics are comprehensively investigated. This device features a remarkably simple structure, an extremely high channel to gate coupling, a large transconductance, and a high current level. Besides, it has the advantage of being based on polymers. This ensures favorable physical properties, ease of fabrication, and low-cost processing techniques.**

***Index Terms*— Conductive polymer matrix composite (CPMC), FET, quantum transport, the nonequilibrium Green's function (NEGF), tunneling.**

I. Introduction

SINCE their advent, conductive polymer matrix composites (CPMCs) have proved to be functional materials for electronic applications owing to some favorable properties [1]. These materials are prepared by dispersing conducting particles in an inherently insulating polymer and are widely used in embedded capacitors [2], memory devices [3], pressure sensors [4], temperature sensors [5], current limiting devices [6], electromagnetic interference shielding and microwave absorption layers [7], and humidity and chemical sensors [8]. CPMC-based devices offer several advantages in comparison with their inorganic rivals, including easy and low-temperature processing, printability over large areas, simple device structures, optical transparency, and lightweight and mechanical flexibility [3], [9].

In order to analyze and optimize the operation of CPMC devices, a profound knowledge of electronic conduction mechanism in CPMCs is required. To date, a great deal of experimental [10], [11] and theoretical [12], [13] work has been performed in order to study the overall system conductivity. The theoretical studies are primarily based on a percolation-tunneling model [13], [14], where the conducting particles are randomly dispersed in the polymer matrix, and they focus on the formation of continuous conducting paths linking the electrodes [14]. These studies have successfully explained the sudden rise in the conductivity and insulator–conductor transition when the filler volume fraction exceeds a definite value called percolation threshold [12]–[14].

Studies revealed that conductivity is of a tunnel nature and current is carried by the electrons tunneling from one conducting island to the other. In other words, the conducting particles are not in direct contact with each other and a potential barrier is developed by the polymer film that is sandwiched between them. An experimental proof to this was provided in [15], where it was shown that the highest conductivity of polymer composites is only on the order of 1% of that of the pure bulk conductive materials. Even alignment of the composites using an electric field, which vigorously pushes the particles toward each other, cannot entirely eliminate this polymer gap [16]. Concerning the tunneling phenomenon, in most theoretical studies, semiclassical relations, such as the ones derived in [17] and [18], using the Wentzel–Kramers–Brillouin (WKB) approximation, are employed [12], [19] and others make use of a simple exponential relation [13], [14].

So far, few studies have been carried out on the potential barriers developed by polymer layers between the particles and the electron transport through them. In this paper, we address these issues by employing a rigorous quantum mechanical approach. Nonequilibrium Green's function (NEGF) formalism is used for this purpose. NEGF method is widely employed to model novel FETs, such as graphene [20]–[22], carbon nanotube [23], [24], and silicon nanowire [25], [26] FETs.

We study the barrier shapes broadly used in literature and the WKB approximation for a wide range of barrier thicknesses, barrier heights, and applied voltages. The results are benchmarked with the quantum mechanical results together

Manuscript received December 4, 2014; accepted March 7, 2015. Date of publication March 27, 2015; date of current version April 20, 2015. The review of this paper was arranged by Editor I. Kymissis.

N. S. Azar is with the School of Electrical and Computer Engineering, University of Tehran, Tehran 14155-8473, Iran (e-mail: n.azar@ut.ac.ir).

M. Pourfath is with the School of Electrical and Computer Engineering, University of Tehran, Tehran 14395-515, Iran, and also with the Institute for Microelectronics, Technische Universität Wien, Wien 1040, Austria (e-mail: pourfath@iue.tuwien.ac.at; pourfath@ut.ac.ir).

Color versions of one or more of the figures in this paper are available online at http://ieeexplore.ieee.org.

Digital Object Identifier 10.1109/TED.2015.2411992

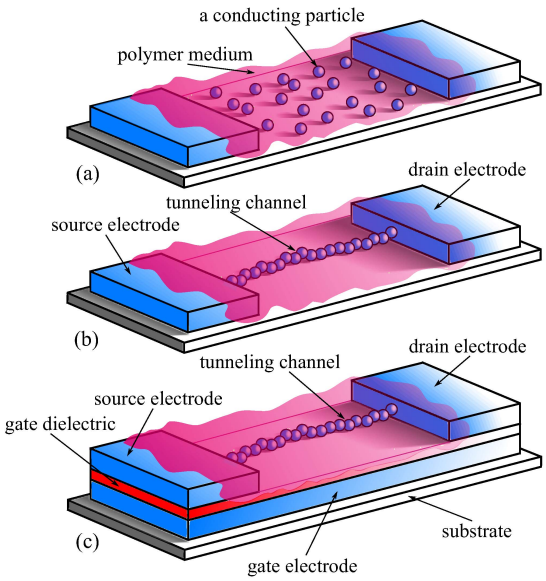

Fig. 1. (a) Device with randomly dispersed particles. (b) Gate-less resistive device. The same device as (a) with an aligned channel formed through electric field alignment before the polymer curing. (c) Gated field-effect device.

with hyperbolic barriers. In addition, there exists little information on the barrier thickness in the literature. Comparing the existing experimental findings [15], [16], [27] with those obtained in this paper, one can draw notable conclusions on the barrier thickness between the conducting islands and conductor–insulator transition. The proposed approach toward the transport phenomena in CPMCs enables us to introduce and investigate the characteristics of a new FET. To the best of our knowledge, such a transistor based on CPMCs has not been introduced before. It is shown that a voltage applied to a third electrode drastically influences the current flowing through the device. In addition to promising electrical characteristics, the proposed device has the advantage of being based on polymers. This ensures favorable physical properties and low-cost fabrication techniques.

II. Approach

It is assumed that electric field alignment [16], [28] is performed during the fabrication of the devices prior to the polymer curing, which results in regular alignment of particles. As a consequence, there exists a continuous path of particles connecting the electrodes, which serves as the channel of the device [Fig. 1(a) and (b)] and percolation effects can be neglected. Alternatively, one can use a filler content higher than the percolation threshold [10], [11], [13], [14], in order to create the tunneling channel needed here; yet, this approach can degrade the physical properties of the material due to the high loading of particles [16]. In this paper, we focus on one aligned channel; however, it can be easily extended to the case with multiple parallel channels.

The electrostatic potential can be obtained by numerically solving Poisson's equation. However, as the charge concentration in the polymer can be safely neglected, an alternative and more computationally efficient approach is taken in this paper. In the case of gate-less resistive devices, shown in Fig. 1(b), the electrostatic potential of the ith conducting island (V_i) is given by

$$V_i = \alpha_i V_{\mathrm{DS}} \tag{1}$$

where V_{DS} is the electric potential applied to the drain electrode and the coefficients α_i are determined by solving Poisson's equation for merely one value of V_{DS}. It should also be noted that the source electrode is grounded in all the simulations. Subsequently, having the potential of conducting islands, the potential distribution between the particles can be evaluated by a linear relation again due to absence of electric charge in the medium.

By adding a third electrode, a novel FET can be obtained. For instance, this can be implemented using a bottom gate structure, as shown in Fig. 1(c). Similar to the previous case and taking advantage of the superposition principle, the electric potential distribution in such devices is calculated. Here, the electric potential of conducting islands are calculated using the relation

$$V_i = \alpha_i V_{\mathrm{GS}} + \beta_i V_{\mathrm{DS}} \tag{2}$$

where α_i and β_i merely depend on the device geometrical parameters and represent the coupling between ith island and the gate and drain electrodes, respectively. These are evaluated by solving Poisson's equation for two values of V_{GS} and V_{DS}. After calculating the potential distribution along the device, the current is evaluated using the Landauer formula

$$I = \frac{2\mathrm{e}}{h} \int T(E)[f_S(E) - f_D(E)]dE \tag{3}$$

where f is the Fermi function, h is Plank's constant, S and D denote the source and drain contacts, and T is the transmission probability through the device. In a device with multiple cascaded barriers, T is expressed as [29, p. 64]

$$\frac{1 - T(E)}{T(E)} = \sum_{i=1}^{N} \frac{1 - T_i(E)}{T_i(E)}. \tag{4}$$

Here, T_i is the transmission probability through the ith barrier (polymer layer between the ith and $(i + 1)$th conducting island) and N is the number of barriers. In fact, the quantity $(1 - T_i)/T_i$ is the resistance attributed to the ith barrier. Scattering rate in metals is rather large, especially scattering caused by electron–electron interaction due to high carrier concentration. Various scattering mechanisms, including electron–electron interaction, can destroy the coherence of electrons [30]. Therefore, coherence between scatterers can be safely neglected here. A similar approach has been applied to model the electron transport through a filamentary-type structure in [31]. $T_i(E)$ for an individual barrier is calculated making use of the NEGF approach [32]

$$T_i(E) = \mathrm{Trace}\left[\Gamma_i G_i \Gamma_{i+1} G_i^{\dagger}\right] \tag{5}$$

where G_i is the Green's function of the ith scatterer, and Γ_i and Γ_{i+1} are the broadenings attributed to the two conducting islands encapsulating the ith polymer barrier.

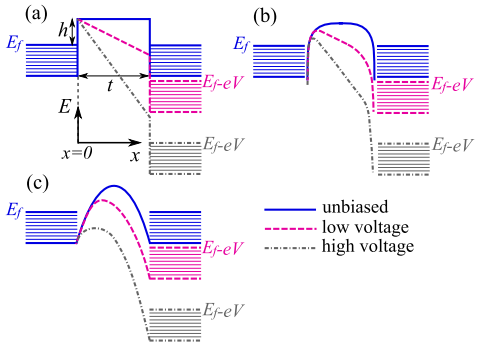

Fig. 2. (a) Rectangular, (b) hyperbolic, and (c) parabolic potential barriers for unbiased, small bias voltage, and high bias voltage conditions, respectively.

An alternative method that is widely used in the literature is the WKB approximation [12], [17]–[19], [33], [34]

$$T_i(E) \approx \exp\left(-\frac{4\pi}{\mathrm{h}} t\sqrt{2\mathrm{m}(\phi_{\mathrm{av}} - E)}\right). \tag{6}$$

Here, ϕ_{av} is the mean barrier height and t is the barrier thickness.

In general, transport equations should be solved in three-dimension; however, it is computationally expensive and the results will strongly depend on the exact geometry of conducting particles. In this paper, T_i is calculated for a 1-D structure and it is assumed that electrons move on a single line connecting the centers of the particles. From another point of view, the 3-D structure can be considered as numerous 1-D structures. As a result, this model can be easily extended to realistic devices without loosing the generality of the results and discussions.

III. Potential Barrier Profiles

Various barrier shapes, such as rectangular [17], [18], parabolic [31], [35], and hyperbolic [17], [33], have been used in the study of tunneling. Fig. 2 shows these barriers for unbiased, low-voltage, and high-voltage conditions. The mentioned potential profiles are given by the following relations.

1) Rectangular barrier [Fig. 2(a)]

$$E(x) = \phi - \mathrm{eV}(x). \tag{7}$$

2) Hyperbolic barrier [Fig. 2(b)] [17]

$$E(x) = \phi - \mathrm{eV}(x) - \frac{1.15\lambda t^2}{x(t-x)} \tag{8}$$

$$\lambda = \frac{e^2 \ln 2}{8\pi t \epsilon}. \tag{9}$$

3) Parabolic barrier [Fig. 2(c)]

$$E(x) = \frac{4}{t^2}\phi(tx - x^2) - \mathrm{eV}(x). \tag{10}$$

Here, in the absence of external field, E_f is an electrode Fermi level that is set to 5.49 eV (Fermi energy of silver [36, p. 12–233]), h is the barrier height from the electrode Fermi level, ϕ equals $E_f + h$, t is the barrier thickness, and ϵ is the permittivity of the barrier. In most simulations,

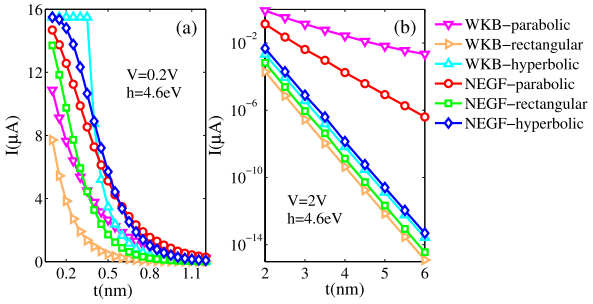

Fig. 3. Current as a function of the barrier thickness for various barrier shapes using the NEGF method and the WKB approximation for (a) thin barriers (linear scale) and (b) thick barriers (logarithmic scale).

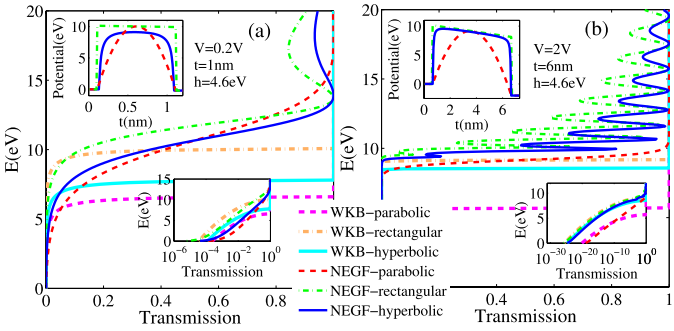

Fig. 4. Potential profile and the spectrum of the transmission for single barriers. The results for (a) thin barrier and (b) thick barrier.

the barrier height is approximated by the work function of the conducting particles (4.6 eV for silver [36, p. 12–124]) as used in [12], [19], and [34]. A hyperbolic barrier is the best choice to model the physical effects at the conductor–insulator interface since it includes image forces [17], [18], [33]. Yet in some studies, rectangular and parabolic shapes are preferred for obtaining simple analytical models [17], [18], [31], [35].

Fig. 3 shows the current as a function of the barrier thickness for each of the barrier shapes employing the NEGF method and the WKB approximation. For a better comparison, Fig. 4 shows the transmission probability for these potential profiles with a thin and also a thick barrier. The results illustrate that the parabolic barrier overestimates the current especially for thick barriers. The rectangular barrier seems to be a more reasonable approximation to hyperbolic; however, it underestimates the current because it neglects the image forces, which effectively lowers the barrier height and thickness. WKB approximation appears to deviate notably from the results of the NEGF, at thick barriers when the parabolic shape is used.

Fig. 5(a) and (b) compares the current as a function of voltage for various potential shapes. For thin barriers, a nearly linear relation between current and voltage is observed, while for thicker barriers the relation deviates from a linear one. In addition to the current overestimation by the parabolic barrier, at higher voltages, the WKB significantly overestimates the current. This behavior is due to the reduction of the effective barrier height and thickness under large bias voltages. In other words, by increasing the voltage, the current–voltage characteristic obtained using the WKB approximation, rapidly

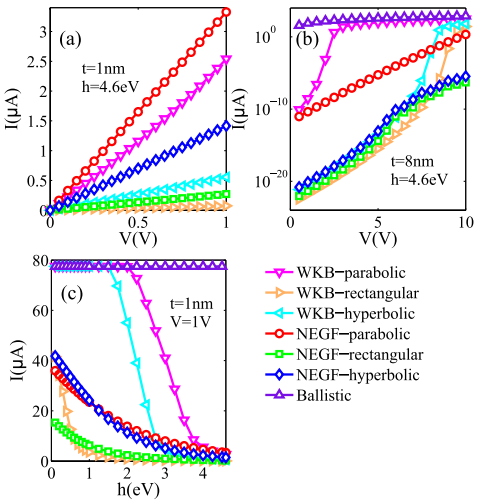

Fig. 5. Current–voltage characteristics for (a) thin barrier, (b) thick barrier, and (c) dependence of the current on the barrier height. All results are for single barriers.

approaches that of the ballistic device ($T(E) = 1$). As shown in Fig. 5(c), the WKB approximation also fails for small barriers. The WKB current coincides with the ballistic current as the barrier height is reduced. In the rest of this paper, the NEGF method along a hyperbolic potential profile is used for the analysis of CPMC devices.

IV. Material Choice

There are few limitations on the choice of conducting and insulating materials in these devices; however, in order to provide an experimentally traceable study, we assume silver as the material for conductive particles and electrodes. The particles are assumed to be ∼50 nm in diameter because smaller particles may suffer from single electron effects that will cause different electrical characteristics due to charging of conductive islands [37]. On the other hand, larger particles result in larger devices and lower dielectric strength that limits the maximum applied bias [38].

Polydimethylsiloxane (PDMS), a functional polymer for electronic devices, is used as the insulating polymer matrix. In a recent study, a breakdown field of 0.635 V/nm has been reported for a 2-μm thick PDMS film [39]. However, thin dielectric layers exhibit greater dielectric strength than thicker samples of the same material. For instance, the dielectric strength of a 50-Å thick Al_2O_3 film is 1 V/nm; while a 12-Å thick film exhibits a dielectric strength as high as 6 V/nm [40]. Consequently, a breakdown field of several volts per nanometer is expected for PDMS ultrathin films that are sandwiched between the conducting islands in CPMC-based devices. Yet, in the case of gated devices, a practical approach for further eliminating the electric breakdown probability is to localize the gate electrode in the middle of the channel, because this causes a smoother voltage gradient along the channel.

V. Gate-Less Resistive Devices

Fig. 6(a) compares the current–voltage characteristics of a gate-less resistive device [Fig. 1(b)] and that of a ballistic

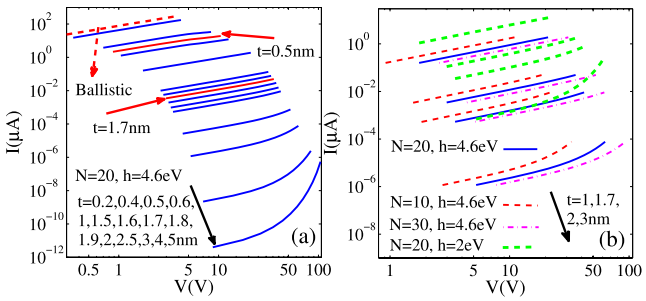

Fig. 6. Current–voltage characteristics of the gate-less resistive devices, illustrating (a) conductor–insulator transition and the minimum barrier thickness and (b) effect of other parameters on conductor–insulator transition. N represents the barrier number ($N - 1$ is the number of conducting particles).

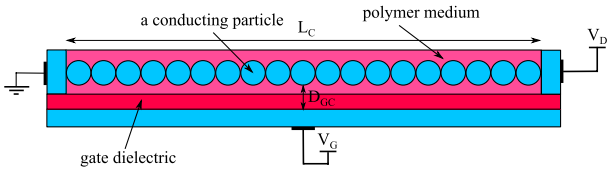

Fig. 7. Sketch of a FET based on CPMCs. L_C stands for channel length and D_{GC} is the gate to channel distance.

device ($T(E) = 1$). It is assumed that all particles are separated with an equal distance. It is observed that for a barrier thickness smaller than ∼1.7 nm, the device shows linear current–voltage curves, which is a characteristic of conductive materials. However, the characteristics become nonlinear for thicker barriers, which is a characteristic of insulating materials. It is, therefore, reasonable to consider $t \approx 1.7$ nm as the critical thickness where conductor–insulator transition occurs in CPMCs. These values are in agreement with the findings of [19] and [27]. As mentioned in Section I, the largest experimentally reported conductivity of polymer composites is nearly 1% of that of the pure bulk conductive materials. Assuming that the pure bulk conductive material is a ballistic conductor, 1% of the conductivity occurs at $t \approx 0.5$ nm for $N = 20$ and $h = 4.26$ eV [Fig. 6(a)]. The size of a polymer molecule is ∼0.5 nm; therefore, regardless of the alignment details, at least a few polymer molecules reside between the conducting particles.

Considering Fig. 6(b), it is perceived that increasing the number of particles slightly reduces the current level. However, it does not influence the linearity of the curves. Besides, as the barrier height reduces, the current level increases but again it does not impact the linearity of the characteristics. Consequently, one can draw the conclusion that the characteristics linearity and conduction behavior of the material solely depend on the barrier thickness.

VI. Gated Devices

Fig. 7 shows the sketch of the simulated device. Fig. 8 shows the output and transfer characteristics of a device with perfectly aligned conducting particles that are 1 nm apart. Fig. 8(a) shows that depending on the gate voltage, the current can be higher or lower than the gate-less counterpart. The well-known operating regions of a FET, triode, and saturation, are observed as well.

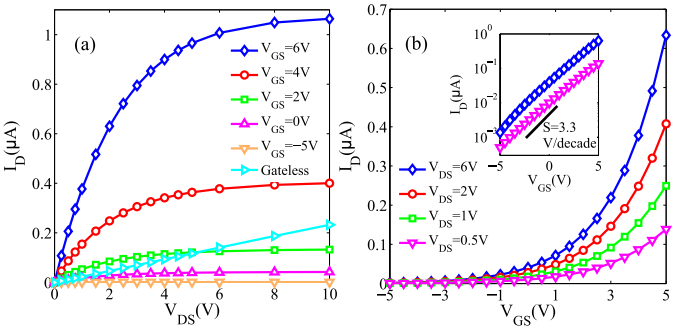

Fig. 8. (a) Output characteristics and (b) transfer characteristics of the FET. The device consists of 50, perfectly aligned particles, where $L_C \approx 2.5$ μm, $t = 1$ nm, and $D_{\mathrm{GC}} = 25$ nm.

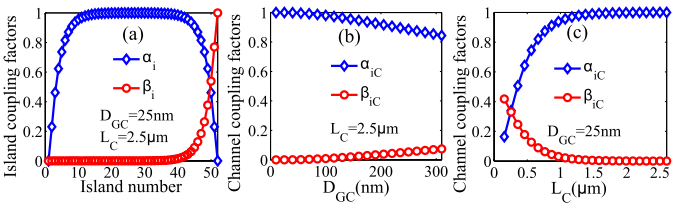

Fig. 9. (a) Island coupling factors of a typical device. The channel coupling factors as a function of (b) gate-channel distance and (c) channel length ($t = 1$ nm).

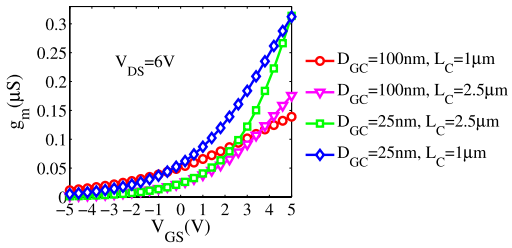

Fig. 10. Transconductance as a function of the gate voltage for various device geometries ($t = 1$ nm).

Fig. 9(a) shows the α_i and β_i factors in the same device. Fig. 9(b) and (c) shows the channel to gate and drain coupling factors as functions of gate-channel distance and channel length, respectively. Here, iC is the island in the middle of the channel, whose coupling factors provide a criterion for determining the device field-effect efficiency. Fig. 9 shows that gate-channel coupling degrades by an increase in the gate-channel distance and a decrease in channel length. For a well-designed device, α_{iC} is much larger than β_{iC} that suggests a high field-effect performance.

Fig. 10 demonstrates the transconductance ($g_m = dI_D/dV_{\mathrm{GS}}$) of a gated device. As mentioned in Section II, the results are only for a 1-D tunneling line and taking a real 3-D structure into account, a high current level, and consequently transconductance can be expected for this device.

VII. Role of Disorder

In Section VI, the particles were assumed to be perfectly aligned and uniformly separated by 1 nm. In a real device, however, some misalignments despite a drastic electric field

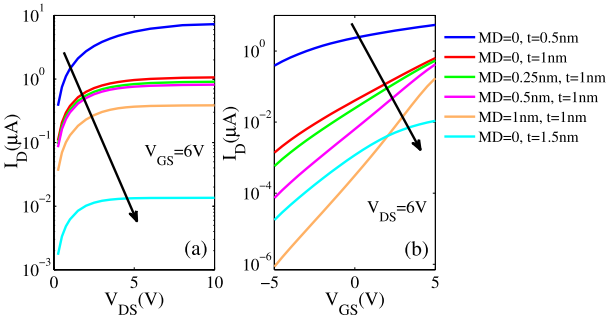

Fig. 11. (a) Output characteristics and (b) transfer characteristics of perfectly and partially aligned devices (50 particles, $L_C \approx 2.5$ μm and $D_{\mathrm{GC}} = 25$ nm).

alignment can occur. In order to investigate the effects of such misalignments, devices with partial alignment of particles are studied in this section. The particles are dispersed randomly using a Gaussian distribution function with maximum deviations of 0.25, 0.5, and 1 nm relative to their initial locations. Fig. 11 compares the output and transfer characteristics for perfectly aligned devices with uniform barrier thicknesses of 0.5, 1, and 1.5 nm and partially aligned devices. In the case of partially aligned devices, numerous devices with random particle locations are simulated for each deviation value and the ensemble average characteristics are shown in the figures. Misalignment causes a drop in the current level, yet it does not disrupt the field-effect behavior of the device. The reduction in current is due to the thicker barriers caused by misalignment and is proportional to the misalignment extent.

VIII. Conclusion

This paper provides a comprehensive study of electron transport in CPMCs from a rigorous quantum mechanical point of view. A benchmarking is made between different barrier shapes as well as the WKB approximation against the accurate quantum mechanical approach in conjunction with a hyperbolic barrier. It is shown that these approximataions, which are widely used in literature, fail for a wide range of barrier parameters. With a detailed study of resistive devices, the conductor–insulator transition and the minimum barrier thickness existing between the conducting sites have been obtained. A novel FET based on CPMCs is introduced and analyzed. This device exhibits promising characteristics, including strong channel-gate coupling, a large transconductance, ease of fabrication, and favorable mechanical properties.

References

[1] J. M. Thomassin, C. Jerome, T. Pardoen, C. Bailly, I. Huynen, and C. Detrembleur, "Polymer/carbon based composites as electromagnetic interference (EMI) shielding materials," *Mater. Sci. Eng., R, Rep.*, vol. 74, no. 7, pp. 211–232, 2013.

[2] L. Qi, B. I. Lee, S. Chen, W. D. Samuels, and G. J. Exarhos, "High-dielectric-constant silver–epoxy composites as embedded dielectrics," *Adv. Mater.*, vol. 17, no. 14, pp. 1777–1781, 2005.

[3] M. Xie, K. C. Aw, M. Langlois, and W. Gao, "Negative differential resistance of a metal–insulator–metal device with gold nanoparticles embedded in polydimethylsiloxane," *Solid State Commun.*, vol. 152, no. 10, pp. 835–838, 2012.

[4] G. Canavese, S. Stassi, M. Stralla, C. Bignardi, and C. F. Pirri, "Stretchable and conformable metal–polymer piezoresistive hybrid system," *Sens. Actuators A, Phys.*, vol. 186, pp. 191–197, Oct. 2012.

[5] G. Matzeu, A. Pucci, S. Savi, M. Romanelli, and F. Di Francesco, "A temperature sensor based on a MWCNT/SEBS nanocomposite," *Sens. Actuators A, Phys.*, vol. 178, pp. 94–99, May 2012.
[6] A. Rybak, G. Boiteux, F. Melis, and G. Seytre, "Conductive polymer composites based on metallic nanofiller as smart materials for current limiting devices," *Compos. Sci. Technol.*, vol. 70, no. 2, pp. 410–416, 2010.
[7] A. Saib *et al.*, "Carbon nanotube composites for broadband microwave absorbing materials," *IEEE Trans. Microw. Theory Techn.*, vol. 54, no. 6, pp. 2745–2754, Jun. 2006.
[8] M. A. Ryan, A. V. Shevade, H. Zhou, and M. L. Homer, "Polymer–carbon black composite sensors in an electronic nose for air-quality monitoring," *MRS Bull.*, vol. 29, no. 10, pp. 714–719, 2004.
[9] Z.-M. Dang, J.-K. Yuan, J.-W. Zha, T. Zhou, S.-T. Li, and G.-H. Hu, "Fundamentals, processes and applications of high-permittivity polymer–matrix composites," *Prog. Mater Sci.*, vol. 57, no. 4, pp. 660–723, 2012.
[10] N. Grossiord *et al.*, "Isotactic polypropylene/carbon nanotube composites prepared by latex technology: Electrical conductivity study," *Eur. Polym. J.*, vol. 46, no. 9, pp. 1833–1843, 2010.
[11] I. A. Tchmutin, A. T. Ponomarenko, E. P. Krinichnaya, G. I. Kozub, and O. N. Efimov, "Electrical properties of composites based on conjugated polymers and conductive fillers," *Carbon*, vol. 41, no. 7, pp. 1391–1395, 2003.
[12] J. Hicks, A. Behnam, and A. Ural, "A computational study of tunneling-percolation electrical transport in graphene-based nanocomposites," *Appl. Phys. Lett.*, vol. 95, no. 21, p. 213103, 2009.
[13] G. Ambrosetti, I. Balberg, and C. Grimaldi, "Percolation-to-hopping crossover in conductor-insulator composites," *Phys. Rev. B, Condens. Matter*, vol. 82, no. 13, p. 134201, 2010.
[14] G. Ambrosetti, C. Grimaldi, I. Balberg, T. Maeder, A. Danani, and P. Ryser, "Solution of the tunneling-percolation problem in the nanocomposite regime," *Phys. Rev. B, Condens. Matter*, vol. 81, no. 15, p. 155434, 2010.
[15] D. Untereker, S. Lyu, J. Schley, G. Martinez, and L. Lohstreter, "Maximum conductivity of packed nanoparticles and their polymer composites," *ACS Appl. Mater. Interf.*, vol. 1, no. 1, pp. 97–101, 2009.
[16] G. K. Johnsen, M. Knaapila, Ø. G. Martinsen, and G. Helgesen, "Conductivity enhancement of silver filled polymer composites through electric field alignment," *Compos. Sci. Technol.*, vol. 72, no. 15, pp. 1841–1847, 2012.
[17] J. G. Simmons, "Generalized formula for the electric tunnel effect between similar electrodes separated by a thin insulating film," *J. Appl. Phys.*, vol. 34, no. 6, pp. 1793–1803, 1963.
[18] R. Holm, "The electric tunnel effect across thin insulator films in contacts," *J. Appl. Phys.*, vol. 22, no. 5, pp. 569–574, 1951.
[19] C. Li, E. T. Thostenson, and T.-W. Chou, "Dominant role of tunneling resistance in the electrical conductivity of carbon nanotube–based composites," *Appl. Phys. Lett.*, vol. 91, no. 22, p. 223114, 2007.
[20] A. Y. Goharrizi, M. Pourfath, M. Fathipour, and H. Kosina, "Device performance of graphene nanoribbon field-effect transistors in the presence of line-edge roughness," *IEEE Trans. Electron Devices*, vol. 59, no. 12, pp. 3527–3532, Dec. 2012.
[21] S.-K. Chin, D. Seah, K.-T. Lam, G. S. Samudra, and G. Liang, "Device physics and characteristics of graphene nanoribbon tunneling FETs," *IEEE Trans. Electron Devices*, vol. 57, no. 11, pp. 3144–3152, Nov. 2010.
[22] N. Ghobadi and M. Pourfath, "A comparative study of tunneling FETs based on graphene and GNR heterostructures," *IEEE Trans. Electron Devices*, vol. 61, no. 1, pp. 186–192, Jan. 2014.
[23] S. O. Koswatta, S. Hasan, M. S. Lundstrom, M. P. Anantram, and D. E. Nikonov, "Nonequilibrium Green's function treatment of phonon scattering in carbon-nanotube transistors," *IEEE Trans. Electron Devices*, vol. 54, no. 9, pp. 2339–2351, Sep. 2007.
[24] G. Fiori, G. Iannaccone, and G. Klimeck, "A three-dimensional simulation study of the performance of carbon nanotube field-effect transistors with doped reservoirs and realistic geometry," *IEEE Trans. Electron Devices*, vol. 53, no. 8, pp. 1782–1788, Aug. 2006.
[25] C. Buran, M. G. Pala, M. Bescond, M. Dubois, and M. Mouis, "Three-dimensional real-space simulation of surface roughness in silicon nanowire FETs," *IEEE Trans. Electron Devices*, vol. 56, no. 10, pp. 2186–2192, Oct. 2009.
[26] N. D. Akhavan *et al.*, "Influence of elastic and inelastic electron–phonon interaction on quantum transport in multigate silicon nanowire MOSFETs," *IEEE Trans. Electron Devices*, vol. 58, no. 4, pp. 1029–1037, Apr. 2011.
[27] C. Fang-Gao, Y. Feng, W. Shao-Xiang, Z. Na, and S. Gui-Lin, "Enhanced piezoresistivity in Ni–silicone rubber composites," *Chin. Phys. B*, vol. 18, no. 2, pp. 652–657, 2009.
[28] C. Park *et al.*, "Aligned single-wall carbon nanotube polymer composites using an electric field," *J. Polym. Sci. B, Polym. Phys.*, vol. 44, no. 12, pp. 1751–1762, 2006.
[29] S. Datta, *Electronic Transport in Mesoscopic Systems*. Cambridge, U.K.: Cambridge Univ. Press, 1997.
[30] S. S. Kahnoj, S. B. Touski, and M. Pourfath, "The effect of electron-electron interaction induced dephasing on electronic transport in graphene nanoribbons," *Appl. Phys. Lett.*, vol. 105, no. 10, p. 103502, 2014.
[31] E. Miranda, A. Mehonic, J. Sune, and A. J. Kenyon, "Multi-channel conduction in redox-based resistive switch modelled using quantum point contact theory," *Appl. Phys. Lett.*, vol. 103, no. 22 p. 222904, 2013.
[32] M. Pourfath, *The Non-Equilibrium Green's Function Method for Nanoscale Device Simulation*. New York, NY, USA: Springer-Verlag, 2014.
[33] W. F. Brinkman, R. C. Dynes, and J. M. Rowell, "Tunneling conductance of asymmetrical barriers," *J. Appl. Phys.*, vol. 41, no. 5, pp. 1915–1921, 1970.
[34] R. L. Jackson and L. Kogut, "Electrical contact resistance theory for anisotropic conductive films considering electron tunneling and particle flattening," *IEEE Trans. Compon., Packag., Manuf. Technol.*, vol. 30, no. 1, pp. 59–66, Mar. 2007.
[35] K. Hansen and M. Brandbyge, "Current-voltage relation for thin tunnel barriers: Parabolic barrier model," *J. Appl. Phys.*, vol. 95, no. 7, pp. 3582–3586, 2004.
[36] D. R. Lide, *CRC Handbook of Chemistry and Physics*. Boca Raton, FL, USA: CRC Press, 2004.
[37] K. K. Likharev, "Single-electron devices and their applications," *Proc. IEEE*, vol. 87, no. 4, pp. 606–632, Apr. 1999.
[38] V. I. Roldughin and V. V. Vysotskii, "Percolation properties of metal-filled polymer films, structure and mechanisms of conductivity," *Prog. Organic Coat.*, vol. 39, nos. 2–4, pp. 81–100, 2000.
[39] A. P. Gerratt and S. Bergbreiter, "Dielectric breakdown of PDMS thin films," *J. Micromech. Microeng.*, vol. 23, no. 6, p. 067001, 2013.
[40] Y. Q. Wu, H. C. Lin, P. D. Ye, and G. D. Wilk, "Current transport and maximum dielectric strength of atomic-layer-deposited ultrathin Al_2O_3 on GaAs," *Appl. Phys. Lett.*, vol. 90, no. 7, p. 072105, 2007.

Nima Sefidmooye Azar received the B.S. degree in electronics from Tabriz University, Tabriz, Iran, in 2013. He is currently pursuing the M.S. degree in electronic devices with Tehran University, Tehran, Iran.

He has been with the Thin Film Laboratory, Tehran University, since 2013. His current research interests include fabrication and modeling of micro and nano-electronic devices and sensors.

Mahdi Pourfath (M'09–SM'15) received the Ph.D. degree in microelectronics from the Technische Universität Wien (TU Wien), Vienna, Austria, in 2007.

He is currently with the School of Electrical and Computer Engineering, University of Tehran, Tehran, Iran, and also with the Institute of Microelectronics, TU Wien. He has authored or co-authored over 120 scientific publications and authored one monograph. His current research interests include novel nanoelectronic devices.